Atmos. Chem. Phys. Discuss., 11, 9607–9633, 2011
www.atmos-chem-phys-discuss.net/11/9607/2011/
doi:10.5194/acpd-11-9607-2011

Atmospheric Chemistry and Physics Discussions

Cloud-base vertical velocity statistics: a comparison between an atmospheric mesoscale model and remote sensing observations

J. Tonttila[1,3], **E. J. O'Connor**[1,2], **S. Niemelä**[1], **P. Räisänen**[1], **and H. Järvinen**[1]

[1]Finnish Meteorological Institute, P.O. Box 503, 00101 Helsinki, Finland
[2]Meteorology Department, University of Reading, Reading, UK
[3]Division of Atmospheric Sciences, Department of Physics, University of Helsinki, Helsinki, Finland

Received: 2 March 2011 – Accepted: 10 March 2011 – Published: 22 March 2011

Correspondence to: J. Tonttila (juha.tonttila@fmi.fi)

Published by Copernicus Publications on behalf of the European Geosciences Union.

Abstract

The statistics of cloud-base vertical velocity simulated by the non-hydrostatic mesoscale model AROME are compared with Cloudnet remote sensing observations at two locations: the ARM SGP site in Central Oklahoma, and the DWD observatory at Lindenberg, Germany. The results show that, as expected, AROME significantly underestimates the variability of vertical velocity at cloud-base compared to observations at their nominal resolution; the standard deviation of vertical velocity in the model is typically 4–6 times smaller than observed, and even more during the winter at Lindenberg. Averaging the observations to the horizontal scale corresponding to the physical grid spacing of AROME (2.5 km) explains 70–80% of the underestimation by the model. Further averaging of the observations in the horizontal is required to match the model values for the standard deviation in vertical velocity. This indicates an effective horizontal resolution for the AROME model of at least 4 times the physically-defined grid spacing. The results illustrate the need for special treatment of sub-grid scale variability of vertical velocities in kilometer-scale atmospheric models, if processes such as aerosol-cloud interactions are to be included in the future.

1 Introduction

The vertical component of atmospheric motions, typically on the order of 1–10 cm s^{-1}, is generally much weaker than its horizontal counterpart, often by 2 orders of magnitude when examined at the synoptic scale. In spite of their relatively small magnitude, vertical motions are necessary in maintaining the global energy cycle and shaping the temperature structure of the atmosphere. In particular, they play a central role in the formation of clouds and precipitation.

Treatment of vertical velocities in atmospheric models, such as numerical weather prediction (NWP) models, varies depending on the assumptions in the model dynamics. NWP models can be divided into two broad classes, hydrostatic and

ACPD
11, 9607–9633, 2011

non-hydrostatic. Hydrostatic models assume hydrostatic balance, where the weight of an air parcel is balanced by the vertical pressure gradient force. This is usually a good approximation at the synoptic scale, and is therefore generally applied in global-scale climate and NWP models. At smaller scales (below 10 km), the hydrostatic assumption becomes increasingly inaccurate and, therefore, many mesoscale NWP and fine-scale models (such as cloud-resolving and large-eddy models) are non-hydrostatic; the vertical velocity tendency is non-zero and a prognostic equation is employed for the vertical wind.

Observations of vertical velocities are important in the development of model parameterizations describing the coupling between atmospheric dynamics and cloud formation and development. Measuring vertical velocities in the atmosphere is difficult, mostly because of their relatively small magnitude. In-situ measurements are, in practice, only possible with research aircraft (Duynkerke et al., 1999; Rodts et al., 2003; Snider et al., 2003; Guo et al., 2008; Lu et al., 2009; Ghate et al., 2010), although mast measurements can be made in layers close to the surface (up to an altitude of a few hundred meters). The aircraft measurements are usually related to intensive field campaigns with limited spatial and temporal coverage, which restricts their usability.

Another measurement technique uses remote sensing by vertically pointing Doppler radars and lidars. These instruments can detect the location of cloud as well as the Doppler velocity. The Doppler velocity is, in this case, related to the vertical motion of atmospheric particles (hydrometeors, aerosols, insects) and can be used to derive estimates of the statistics of atmospheric vertical velocities (e.g. Frisch et al., 1995; Feingold et al., 1999; Kollias and Albrecht, 2000; Kollias et al., 2001; O'Connor et al., 2005; Hogan et al., 2009). As in-situ measurements, the vertically pointing remote sensing observations suffer from poor spatial coverage, but they have the important advantage of being able to measure different layers of atmospheric vertical columns simultaneously with good temporal resolution, which is practically impossible to attain with in-situ measurements. Moreover, some research programmes, such as the Atmospheric Radiation Measurement (ARM) programme (Ackerman and Stokes, 2003) and

ACPD
11, 9607–9633, 2011

Cloudnet (Illingworth et al., 2007) provide long time series of Doppler measurements covering several years from several stations around the world.

In this work we use ground-based vertically-pointing Doppler cloud radar measurements to evaluate the ability of the non-hydrostatic regional NWP model AROME (Seity et al., 2010) to simulate the vertical velocity fields. Our focus is on the magnitude of variability of vertical velocity at the cloud-base. The statistics of the simulated cloud-base vertical velocities are compared with those from ground-based vertically-pointing Doppler cloud radar measurements. In Sect. 2 we describe the instruments that supply the observations, and, in Sect. 3, we outline the pertinent features of the mesoscale model AROME. Data from both sources require further processing to obtain suitable cloud-base vertical velocities for comparison, and this important step is discussed in Sect. 4. The results are reported in Sect. 5 before concluding in Sect. 6.

2 Observations

We analyse observations from two sites with zenith-pointing millimeter-wavelength Doppler cloud radars; the Atmospheric Radiation Measurement (ARM) Southern Great Plains (SGP) site in Central Oklahoma, US (Clothiaux et al., 1999), and the Deutscher Wetterdienst (DWD) observatory in Lindenberg, Germany. Both sites are also equipped with co-located lidars, ceilometers, and complemented by a suite of surface instruments.

To identify suitable targets from which to infer the vertical motion of the air, we use the Cloudnet target classification product (Illingworth et al., 2007), which utilizes Doppler cloud radar, lidar and/or ceilometer, dual-wavelength microwave radiometer, raingauge and NWP model data to distinguish between, and categorize, different types of particles and hydrometeors (such as liquid cloud droplets, ice particles, liquid precipitation, drizzle, insects and aerosol). All instruments are processed and averaged to a common time-height grid with a nominal temporal resolution of 30 s.

ACPD
11, 9607–9633, 2011

The Doppler cloud radar at SGP is the 35 GHz millimeter-wavelength cloud radar, MMCR (Clothiaux et al., 1999), which has a number of operational modes; we therefore use the Active Remote Sensing of Clouds (ARSCL) dataset (Clothiaux et al., 2000, 2001) as input to the Cloudnet processing scheme. The ensuing vertical resolution is approximately 90 m. The Doppler cloud radar at Lindenberg is the 35.5 GHz MIRA and the vertical resolution of the Cloudnet product is approximately 30 m. The intrinsic error in the mean Doppler velocity is smaller than the bin width of the measured Doppler spectrum and, hence, for both Doppler cloud radars, the Doppler velocity resolution is on the order of 2 cm s^{-1}.

Cloudnet processed data from both sites is available for the years 2004–2009; for this paper we have taken the months of January and June and refer to the two datasets from now on as CN-SGP and CN-Lindenberg. The Lindenberg site provides a quite different climatic regime, compared to SGP, offering greater low-cloud occurrence (with more cases of stratiform cloud decks), whereas SGP presents more scattered cloud characteristics.

3 AROME mesoscale model

AROME (Applications of Research to Operations at MEsoscale; Seity et al., 2010) is a limited-area, mesoscale numerical weather prediction model originally designed by Meteo-France. The model is further developed together by the HIRLAM-programme group (10 European countries) and Meteo-France. The model has a non-hydrostatic compressible atmosphere with a semi-Lagrangian advection scheme. The physical parameterizations of the model use a three-dimensional rectangular grid, while the dynamics are solved in spectral space.

The physical parameterizations in AROME are mostly adopted from the MESO-NH model (Lafore et al., 1998). These include a turbulence scheme (Cuxart et al., 2000) providing prognostic turbulent kinetic energy, TKE, and a bulk microphysics scheme with 5 prognostic variables for different water species: cloud water and ice mixing ratios,

ACPD
11, 9607–9633, 2011

and mixing ratios for liquid rain, snowfall and graupel (Pinty and Jabouille, 1998). In addition, AROME has a statistical subgrid cloud scheme based on saturation adjustment, where cloud cover is calculated using a probability density function, whose variance depends on the saturation deficit (Bechtold et al., 1995). Rainfall is described statistically as well, so that the fall speeds of different sized precipitation particles are described by a probability density function (Geleyn et al., 2008). The contribution of shallow, non-precipitating cumulus convection and dry thermals is parameterized in terms of the vertical mass flux and properties in the convective updrafts (as described in Pergaud et al., 2009). The effect of the surface on the atmospheric boundary layer is taken into account via fluxes of momentum, heat and moisture, which are provided by the surface module SURFEX (Le Moigne, 2009). Each grid box is divided into four tiles: land, urban, sea, and inland waters. The fluxes from each tile are then areal-averaged in order to determine the net effect for the whole grid box. The radiation scheme is based on ECMWF's radiation code (Fouquart and Bonnel, 1980; Morcrette, 1991; Mlawer et al., 1997).

3.1 Model setup

The model was run with domains centred on each observation site (300 × 300 grid points for the SGP domain, 160 × 160 gridpoints for the Lindenberg domain), providing 12-h forecasts with output at 3-hourly intervals. For both domains, analyses from the operational Integrated Forecasting System (IFS) at ECMWF were used to provide the initial model state, and lateral boundary conditions were updated every 6 h from IFS forecasts. For both experiments, the horizontal resolution of the model was 2.5 km, with a 60 s time step. Vertical discretization uses terrain-following hybrid coordinates (40 levels) with a resolution of approximately 30 m close to the surface, gradually increasing to a few hundred meters through the troposphere (8 levels within the lowest 1000 m). With a 2.5 km grid spacing, large convective flow structures are assumed to be resolved explicitly and, therefore, the parameterization for deep convection was not switched on for this particular model configuration. Model output was generated for the months of

ACPD
11, 9607–9633, 2011

January and June; at SGP for 2007 and 2008, and at Lindenberg, for 2008 only.

4 Determination of cloud-base vertical velocity

This section focuses on the assessment of the probability density function (PDF) of cloud-base vertical velocity, and its variance, as retrieved from the AROME and the CloudNet datasets. The goal is to provide a simple evaluation of the statistical aspects of model-generated vertical velocities at cloud base.

4.1 Model data

There is no unique approach to determine cloud boundaries and cloud-base vertical velocities from model data. In this study, a threshold value for the AROME grid-cell fractional cloudiness is used. The cloud base height is taken as the altitude of the lowest model level containing liquid cloud water only and with a cloud fraction value exceeding 0.5. Ice-phase, mixed-phase and precipitating cloud layers are discarded from the analysis in order to match the data processing in the model and the observations as described in Sect. 4.2. Only the base of the lowest cloud layer in each grid column is taken into consideration.

After determining the cloud-base level using the criteria above, the cloud-base vertical velocity is taken from the corresponding grid-point value of vertical velocity. The cloud fraction value at cloud-base is used as a weighting factor in the calculation of the vertical velocity statistics. Because the fractional cloudiness values are usually close to 0 or 1 for the 2.5 km grid of AROME, with only a relatively small number of grid points having intermediate values, the effect of these weighting factors is relatively weak. Additionally, the U-shaped distribution of cloud fraction values in this model facilitates the use of a cloud fraction threshold of 0.5 for cloud detection; the results are not sensitive to the actual threshold value chosen.

ACPD
11, 9607–9633, 2011

4.2 Observations

The use of Doppler velocity measurements as a surrogate for the vertical air motion is vulnerable to biases caused by incorrectly including values from targets that have an appreciable terminal velocity. We attempt to minimize these biases by careful inspection and selection of data.

Liquid cloud droplets (with diameters on the order of about 10 µm) typically have very low terminal falling velocities on the order of few centimeters per second (e.g. Rogers, 1976; Kollias et al., 2001; Khvorostyanov and Curry, 2002). If we limit our considerations to observations with only liquid cloud droplets present, the use of Doppler velocity as a proxy for the vertical air velocity can be justified. The Doppler velocities from cloud bases where rain, drizzle, or ice is also present must be discarded as these hydrometeors have significant terminal velocities. Likewise, small insects are not passive tracers and their mean vertical motion can exhibit significant bias (Geerts and Miao, 2005). These targets are identified within the Cloudnet classification product, which is then used to identify the lowest observed suitable liquid cloud base height and, hence, the cloud base vertical velocity (taken as the mean Doppler velocity at this altitude).

To illustrate the necessity of removing unwanted targets we concentrate briefly on the results for one day, 6th June 2008, at Lindenberg. The Cloudnet classification product for this day is given in Fig. 1, displaying the various targets identified for a liquid layer lying close to the freezing level (potentially supercooled), including rain, drizzle and ice. Two segments of data have been sampled to produce cloud-base vertical velocity distributions; one from 09:00 UTC to 15:00 UTC containing drizzle (and rain and ice cloud events) interspersed with drizzle-free liquid layers; and one from 18:00 UTC to 24:00 UTC that is completely drizzle-free. The vertical velocity distribution for the completely drizzle-free segment, given in Fig. 2a, is reasonably symmetric about 0 m s^{-1}. For the segment which includes additional targets, two vertical velocity distributions are produced. Figure 2b contains cloud-base vertical velocity values where drizzle coexists within, or is detected below, the liquid layer. Figure 2c contains, in addition to

ACPD
11, 9607–9633, 2011

drizzle, vertical velocity values where ice co-exists within, or is detected just above, the liquid layer. Figure 2b,c shows an obvious negative velocity bias and, as expected, a second, strongly negative, mode. One direct consequence is a significant broadening of the distribution, clearly displaying the effect of large hydrometeors on the vertical velocity distribution. If not detected and removed, drizzle will therefore increase the risk of bias in the results.

Drizzle is, in fact, a serious concern and can be difficult to detect in-cloud. As an additional precaution, a maximum threshold for radar reflectivity is used. Earlier studies have employed thresholds, such as −17 dB Z (Frisch et al., 1995; Feingold et al., 1999; Ghate et al., 2010), to delineate drizzle from drizzle-free clouds, but, since our interest is specifically on the vertical velocities at cloud base, where cloud droplets are at their smallest and drizzle drops presumably at their largest, a maximum value of −30 dB Z is used in this study (see Liu et al., 2008; Kollias and Albrecht, 2010). These constraints limit our investigation to a rather small fraction of the total number of observed liquid cloud layers.

5 Results

5.1 Direct comparison with observations

The vertical velocities at cloud base from both AROME and Cloudnet datasets are apportioned into 500 m bins according to altitude. The lowest cloud base height bin is 500–1000 m while the highest is limited to around 3500–4000 m (2000–2500 m during winter), because the number of observations with liquid cloud droplets decreases rapidly at higher altitudes. Figures 3 and 4 illustrate cloud base vertical velocity histograms from SGP and Lindenberg in January for a single cloud base altitude bin (between 1000 and 1500 m). These are representative of typical differences between modelled (AROME) and observed (Cloudnet) velocity distributions. The vertical velocity histograms from AROME are quite narrow (standard deviation of about 0.1 m s^{-1} at both

ACPD
11, 9607–9633, 2011

sites), with a slight positive skewness (similar to results found by Zhu and Zuidema, 2009) and a mean close to zero. In contrast, the observed vertical velocities exhibit much wider distributions at both sites (standard deviation of about 0.4–0.5 m s^{-1}). The observations tend to show a slight preponderance towards negative velocities, leading to a negative mean value in the distribution. The velocity distributions at all altitudes are qualitatively similar (not shown).

Figure 5 displays the mean and standard deviation of the vertical velocity distribution as a function of height for January and June at SGP and Lindenberg. In January, the mean vertical velocity in AROME is very close to zero in both domains. This is also true in June for Lindenberg, while for SGP, AROME now displays positive mean values, although still below 0.1 m s^{-1}. In contrast, the observations show a consistent negative mean value, typically −0.2 m s^{-1}, at all heights and for both January and June, although values as low as −0.4 m s^{-1} are seen at SGP in January close to the surface. Since the vertical velocity averages are expected to approach zero (or slightly positive values in cloud) over a long period of time, the negative mean value most likely represents a bias due to occasional large hydrometeors or other particles (as discussed in Frisch et al., 1995; Kollias and Albrecht, 2000; O'Connor et al., 2005), where the associated velocities have not been rejected even after the strict qualification for the selection of drizzle-free cloud-base vertical velocities.

Of potentially more importance is the variabilility in vertical velocity at cloud-base, here investigated by taking the standard deviation of the vertical velocity distributions, σ_w. It is immediately clear from Fig. 5 that the observed values of σ_w are always larger than their corresponding model values. In January, the observed σ_w values range from 0.4–0.5 m s^{-1}, while the model values are 0.05–0.10 m s^{-1}. AROME thus underestimates σ_w typically by a factor of 4–6 in January. At Lindenberg in June, the observed σ_w is slightly larger (0.5–0.6 m s^{-1}), while σ_w in AROME is similar to January values. At SGP in June, the observed σ_w is 0.8–1.0 m s^{-1} consistently across all altitudes. The σ_w values in AROME at SGP in June are also much larger, from 0.1 m s^{-1} close to the surface, to 0.4 m s^{-1} at higher altitudes. In June, AROME thus underestimates σ_w by

ACPD
11, 9607–9633, 2011

a factor of 2 – –5 at SGP, whereas the underestimation at Lindenberg, is by a factor of 5–6, and in the worst case almost by a factor 10.

5.1.1 Effect of bias on the comparison of σ_w

The direct comparison of σ_w does not account for the negative bias in the observations. To investigate how the bias affects this comparison, we next calculate the root mean square (RMS) values separately for the positive (RMS+) and negative (RMS−) portions of the vertical velocity distributions. By this experiment we attempt to show that the negative bias in the observations does not significantly alter the shape of the distribution and, most importantly, the value of σ_w. If we assume that the negative bias is a true bias and affects the entire distribution equally, we would then expect the observed RMS− to be consistently larger than the observed RMS+. In contrast, RMS+ values from unbiased model velocity distributions should be larger than, or similar, to RMS− values.

Figure 6 shows that this is indeed the case. Profiles of RMS− and RMS+ are plotted for the modelled and observed velocity distributions over both domains for the months of January and June. In January, the observed RMS− is consistently 50% or so larger than the observed RMS+ at both sites, whereas the model RMS− is usually smaller than RMS+ (the model has a slightly positive tail in the cloud base vertical velocity distribution). Observed magnitudes of RMS are much larger than their model counterparts, a consequence of the much larger observed values of σ_w (Fig. 5). The same results are true for Lindenberg in June.

The results are markedly different at SGP in June. In a more convective environment, the model values for RMS+ are not only large (as might be expected from the σ_w values shown in Fig. 5), but considerably larger than RMS−; this is directly attributable to the cloud-scheme predicting cumulus in updrafts only. The observations do not display the same pattern, even after taking into account the likely effect of the negative bias, as the observed RMS− is still at least 50% larger than the observed RMS+.

ACPD
11, 9607–9633, 2011

Theoretically, a normal distribution with a mean of $-0.2\,\mathrm{m\,s^{-1}}$ and $\sigma_w = -0.5\,\mathrm{m\,s^{-1}}$ should result in RMS− being larger than RMS+ by a factor of about 1.5, similar to what is seen in practice. This suggests that we can assume that the bias has had little impact on the distribution shape, however, with the important caveat that the observed velocity distribution may not necessarily conform to the ideal.

5.2 Comparison with observations averaged to the model resolution

It is clear that much of the variability of cloud-base vertical velocity is at scales that AROME does not resolve. To investigate which horizontal scales the model is capable of resolving we undertake a case study where the observed time-height cross-sections of vertical velocity are averaged onto different horizontal spatial scales.

The averaging is performed by first converting the time increments in the observations into spatial distances using the horizontal wind velocity from AROME at each height as an advection speed. The scales selected for averaging range from 500 m to 10 km. Finding long segments of continuous stratiform cloud decks is a prerequisite for calculating the averages over the desired length scales, while concurrently producing enough data to derive confident statistics. Moreover, as before, we are forced to limit our considerations to clouds with only liquid droplets. Only a handful of such realizations were covered by both the model data and observations. In Figs. 7 and 8, we present the best case, comprising data from Lindenberg for 29–30 January 2008. During this period, the cloud-base altitude varied from 1000 m to 1500 m. Figure 7 illustrates the effect of averaging on the shape of the distribution of cloud-base vertical velocities, where observations averaged to the 2500 m scale are compared to the observations at their original resolution, and AROME. Figure 8 shows how the observed σ_w, calculated from distributions including those in Fig. 7, behaves as a function of the averaging length scale. It is evident that σ_w appears to decrease almost exponentially with increasing averaging length. In particular, at the 2500 m scale, corresponding to the physical grid spacing of AROME, σ_w is approximately $0.21\,\mathrm{m\,s^{-1}}$, being about 60%

ACPD
11, 9607–9633, 2011

smaller than the observed σ_w for data at the original resolution (0.51 m s^{-1}).

The result shows that averaging to the physical grid spacing of AROME is not enough to explain all of the underestimation of σ_w in the model, and that, according to Fig. 8, an averaging scale of 10 km is required for the observations to produce values comparable with the model. Thus, the grid point values in AROME should be considered to be representative of an effective horizontal resolution rather than the physical grid spacing, as described in Skamarock (2004) through the use of kinetic energy spectra. Depending on the treatment of kinetic energy dissipation at the smallest scales represented by the model, the effective resolution can be expected to be around 4–8 times the nominal grid spacing. Therefore, obtaining statistics comparable with AROME at an averaging scale of 10 km, as seen in Fig. 8, is actually close to what we would expect.

6 Discussion and conclusions

The statistics of the vertical velocity fields simulated by the AROME numerical weather prediction model were compared with the vertically pointing Doppler radar observations at two sites, the Atmospheric Radiation Measurement programme Southern Great Plains (SGP) site (Oklahoma, US) and Lindenberg (Germany). At these two sites, the model mean cloud-base vertical velocity is very close to zero during winter and the standard deviation of cloud-base vertical velocity, σ_w, is also very similar. A mean vertical velocity close to zero is seen also in summer at Lindenberg in the model data. At SGP, however, a positive mean vertical velocity is found for summer, together with a significant increase in σ_w, attributable to the strong convective nature at this location. Observations at these two sites show a consistent negative, or downwards, bias in the mean cloud-base vertical velocity in both summer and winter, with no shift towards positive values apparent at SGP in summer. We show that the negative bias does not appear to affect the variability estimates from observations, with similar values of σ_w found at both sites in winter, and at Lindenberg in summer. Again, similar to the model data, the observations show a significant increase in σ_w at SGP in summer.

ACPD
11, 9607–9633, 2011

We found that AROME underestimates considerably the variability of vertical velocity, when compared to the observations, with σ_w for the simulated vertical velocity distribution being typically 4–6 times smaller than that of the observed distribution. For the most part, the underestimation is due to the insufficient model resolution: the 2.5 km physical grid spacing of AROME is clearly too coarse to resolve all the details in vertical velocity variations. A portion of cumuliform updraft-downdraft structure will be unresolved as well, since the horizontal scales of updraft cores in cumulus clouds can easily go down to a few hundred meters (Kollias et al., 2001). The influence of grid resolution on the updraft velocities has been noted elsewhere as well; in their extensive large-eddy simulations, Khairoutdinov et al. (2009) reported a significant decrease in the magnitudes of vertical velocities in convective updraft cores as the horizontal grid spacing of the model was increased gradually from 100 m to 1.6 km. Moreover, it has been noted that also the vertical resolution of a model has an effect on the representation of vertical velocities. Guo et al. (2008) suggested that a vertical resolution of about 10 m is needed to robustly resolve the higher order statistical moments of vertical velocities.

The importance of horizontal resolution was studied in the present paper as well by applying a method of averaging to the vertical velocity observations. At the scale of the physical grid spacing of AROME, we found that σ_w from averaged observations was still slightly larger than that in AROME data. This illustrates the fact that the grid point values of vertical velocity in AROME should be considered to represent an effective resolution, rather than the scales of the physical grid spacing of 2.5 km (similar to the results of Skamarock, 2004). As noted in Sect. 5.2, an averaging scale of 10 km was needed for the observations to produce statistics comparable with AROME, which suggests that the effective resolution of AROME is at least 4 times the physical grid spacing of the model. Once this effective resolution was taken into account, the model showed good agreement with the observed distributions of vertical velocity at different locations and in different seasons. This implies that the effective model resolution must be accounted for in any microphysical parameterizations making use of the model

ACPD
11, 9607–9633, 2011

vertical velocity, or other grid point values.

One application for which the correct description of the vertical velocity distribution is required is modelling of aerosol-cloud interactions. The number of cloud droplets formed in an ascending air parcel depends both on the aerosol population and the updraft speed; if the latter is underestimated, the cloud droplet number concentration (CDNC) is underpredicted, too. This problem was noted, e.g., by Ivanova and Leighton (2008), who used a non-hydrostatic model with a 3 km horizontal resolution to simulate the cloud activation of aerosols. When using the grid scale vertical velocities simulated directly by their model, then CDNC was underestimated considerably, and this was ascribed to the underestimation of cloud-base vertical velocities. The study by Ivanova and Leighton (2008) and the present paper both suggest that when the aerosol activation process is simulated in a mesoscale model with a horizontal resolution of a few kilometres, the grid-scale vertical velocities should not be used as such, but rather a parameterization accounting for the subgrid variations of vertical velocity, similar to those developed for general circulation models (Ghan et al., 1997; Lohmann et al., 1999; Hoose et al., 2010), is needed.

Acknowledgements. We acknowledge the Cloudnet project (European Union contract EVK2-2000-00611) for providing the categorization and classification datasets, which was produced by the University of Reading using measurements from Lindenberg, Germany.

The ARSCL dataset was obtained from the Atmospheric Radiation Measurement (ARM) Program sponsored by the US Department of Energy, Office of Science, Office of Biological and Environmental Research, Climate and Environmental Sciences Division.

This work has been supported by the Academy of Finland (project number 127210).

ACPD

11, 9607–9633, 2011

References

Ackerman, T. P., Stokes, G.: The atmospheric radiation measurement program, Phys. Today, 56, 38–44, doi:10.1063/1.1554135, 2003. 9609

Bechtold, P., Cuijpers, J. W. M., Mascart, P., and Trouilhet, P.: Modelling of trade wind cumuli with a low-order turbulence model: toward a unified description of Cu and Sc clouds in meteorological models, J. Atmos. Sci., 52, 455–463, 1995. 9612

Clothiaux, E. E., Moran, K. P., Martner, B. E., Ackerman, T. P., Mace, G. G., Uttal, T., Mather, J. H., Widener, K. B., Miller, M. A., and Rodriguez. D. J.: The atmospheric radiation measurement program cloud radars: operational modes, J. Atmos. Ocean. Tech., 16, 819–827, 1999. 9610, 9611

Clothiaux, E. E., Ackerman, T. P., Mace, G. G., Moran, K. P., Marchand, R. T., Miller, M. A., and Martner, B. E.: Objective determination of cloud heights and radar reflectivities using a combination of active remote sensors at the ARM CART sites, J. Appl. Metorol., 39, 645–665, 2000. 9611

Clothiaux, E. E., Miller, M.A, Perez, R. C., Turner, D. D., Moran, K. P., Martner, B. E., Ackerman, T. P., Mace, G. G., Marchand, R. T., Widener, K. B., Rodriguez, D. J., Uttal, T., Mather, J. H., Flynn, C. J., Gaustad, K. L., and Ermold, B.: The ARM Millimeter Wave Cloud Radars (MMCRs) and the Active Remote Sensing of Clouds (ARSCL) Value Added Product (VAP), DOE Tech. Memo. ARM VAP-002.1, available at: http://www.arm.gov/publications/vaps, last access: 21 March 2011, 2001. 9611

Cuxart, J., Bougeault, P., and Redelsperger, J. L.: A turbulence scheme allowing for mesoscale and large eddy simulations, Q. J. Roy. Meteor. Soc., 126, 1–30, 2000. 9611

Duynkerke, P. G., Jonker, P. J., Chlond, A., Van Zanten, M. C., Cuxart, J., Clark, P., Sanchez, E., Martin, G., Lenderink, G., and Teixeira, J.: Intercomparison of three- and one-dimensional model simulations and aircraft observations of stratocumulus, Bound.-Lay. Meteorol., 92, 453–487, 1999. 9609

Feingold, G., Frisch, A. S., Stevens, B., and Cotton, W. R.: On the relationship among cloud turbulence, droplet formation and drizzle as viewed by Doppler radar, microwave radiometer and lidar, J. Geophys. Res., 104, 22195–22203, 1999. 9609, 9615

Fouquart, Y. and Bonnel, B.: Computations of solar heating of the Earth's atmosphere: a new parameterization, Beitr. Phys. Atmos., 53, 35–62, 1980. 9612

Frisch, A. S., Lenschow, D. H., Fairall, C. W., Schubert, W. H., and Gibson, J. S.: Doppler radar

ACPD
11, 9607–9633, 2011

measurements of turbulence in marine stratiform cloud during ASTEX, J. Atmos. Sci., 52, 2800–2808, 1995. 9609, 9615, 9616
Geerts, B. and Miao, Q.: The use of millimeter doppler radar echoes to estimate vertical air velocities in the fair-weather convective boundary layer, J. Atmos. Ocean. Technol., 22, 225–246, 2005. 9614
Geleyn, J.-F., Catry, B., Bouteloup, Y., and Brozkova, R.: A statistical approach for sedimentation inside a microphysical precipitation scheme, Tellus A, 60, 649–662, 2008. 9612
Ghan, S. J., Leung, L. R., Easter, R. C., and Abdul-Razzak, H.: Prediction of cloud droplet number in a general circulation model, J. Geophys. Res., 102, 21777–21794, 1997. 9621
Ghate, V. P., Albrecht, B. A., and Kollias, P.: Vertical velocity structure of nonprecipitating continental boundary layer stratocumulus clouds, J. Geophys. Res., 115, D13204, doi:10.1029/2009JD013091, 2010. 9609, 9615
Guo, H., Liu, Y., Daum, P. H., Senum, G. I., and Tao, W.-K.: Characteristics of vertical velocity in marine stratocumulus: comparison of large eddy simulations with observations, Environ. Res. Lett., 3, 045020, doi:10.1088/1748-9326/3/4/045020, 2008. 9609, 9620
Hogan, R. J., Grant, A. L., Illingworth, A. J., Pearson, G. N., and O'Connor, E. J.: Vertical velocity variance and skewness in clear and cloud-topped boundary layers as revealed by Doppler lidar, Q. J. Roy. Meteor. Soc., 135, 635–643, 2009. 9609
Hoose, C., Kristjánsson, J. E., Arabas, S., Boers, R., Pawlowska, H., Puygrenier, V., Siebert, H., and Thouron, O.: Parameterization of in-cloud vertical velocities for cloud droplet activation calculations in coarse-grid models: analysis of observations and cloud resolving model results, 13th Conference on Atmospheric Raditation, Portland, OR, USA, 28 June–2 July 2010, Presentation 6.4, available at: http://ams.confex.com/ams/pdfpapers/170866.pdf, last access: 21 March 2011, 2010. 9621
Illingworth, A. J., Hogan, R. J., O'Connor, E. J., Bouniol, D., Brooks, M. E., Delanoë, J., Donovan, D. P., Eastment, J. D., Gaussiat, N., Goddard, J. W. F., Haeffelin, M., Klein Baltink, H., Krasnov, O. A., Pelon, J., Piriou, J.-M., Protat, A., Russchenberg, H. W. J., Seifert, A., Tompkins, A. M., van Zadelhoff, G.-J., Vinit, F., Willén, U., Wilson, D. R., and Wrench, C. L.: Cloudnet: continuous evaluation of cloud profiles in seven operational models using ground-based observations, B. Am. Meteorol. Soc., 88, 883–898, 2007. 9610
Ivanova, I. T. and Leighton, H. G.: Aerosol-cloud interactions in a mesoscale model, part I: sensitivity to activation and collision-coalescence, J. Atmos. Sci., 65, 289–308, 2008. 9621
Khairoutdinov, M. F., Krueger, S. K., Moeng, C.-H., Bogenschutz, P. A., and Randall, D. A.:

ACPD
11, 9607–9633, 2011

Large-eddy simulation of deep maritime tropical convection, J. Adv. Model. Earth Syst., 1(15), 13 pp., 2009. 9620
Khvorostyanov, V. I. and Curry, J. A.: Terminal velocities of droplets and crystals: power laws with continuous parameters over the size spectrum, J. Atmos. Sci., 59, 1872–1884, 2002. 9614
Kollias, P. and Albrecht B.: The turbulence structure in a continental stratocumulus cloud from millimeter-wavelength radar observations, J. Atmos. Sci., 57, 2417–2434, 2000. 9609, 9616
Kollias, P. and Albrecht B.: Vertical velocity statistics in fair-weather cumuli at the ARM TWP Nauru Climate Research Facility, J. Clim., 23, 6590–6604, 2010. 9615
Kollias, P., Albrecht, B., Lhermitte, R., and Savtchenko, A.: Radar observations of updrafts, downdrafts, and turbulence in fair-weather cumuli, J. Atmos. Sci., 58, 1750–1766, 2001. 9609, 9614, 9620
Lafore, J. P., Stein, J., Asencio, N., Bougeault, P., Ducrocq, V., Duron, J., Fischer, C., Héreil, P., Mascart, P., Masson, V., Pinty, J. P., Redelsperger, J. L., Richard, E., and Vilà-Guerau de Arellano, J.: The Meso-NH Atmospheric Simulation System. Part I: adiabatic formulation and control simulations, Ann. Geophys., 16, 90–109, doi:10.1007/s00585-997-0090-6, 1998. 9611
Le Moigne, P.: SURFEX scientific documentation, online documentation available at: http://www.cnrm.meteo.fr/surfex/doc_exter/surfex_scidoc.pdf, last access: 21 March 2011, 2009. 9612
Liu, Y., Geerts, B., Miller, M., Daum, P., and McGraw, R.: Threshold radar reflectivity for drizzling clouds, Geophys. Res. Lett., 35, L03807, doi:10.1029/2007GL031201, 2008. 9615
Lohmann, U., Feichter, J., Chuang, C. C., and Penner, J. E.: Prediction of the number of cloud droplets in the ECHAM GCM, J. Geophys. Res., 104, 9169–9198, 1999. 9621
Lu, M.-L., Sorooshian, A., Jonsson, H. H., Feingold, G., Flagan, R. C., and Seinfeld, J. H.: Marine stratocumulus aerosol-cloud relationships in the MASE-II experiment: precipitation susceptibility in Eastern Pacific marine stratocumulus, J. Geophys. Res., 114, D24203, doi:10.1029/2009JD012774, 2009. 9609
Mlawer, E. J., Taubman, S. J., Brown, P. D., Iacono, M. J., and Clough, S. A.: Radiative transfer for inhomogeneous atmospheres: RRTM, a validated correlated-*k* model for the long wave, J. Geophys. Res., 102, 16663–16682, 1997. 9612
Morcrette, J.-J.: Radiation and cloud radiative properties in the ECMWF operational weather forecast model, J. Geophys. Res., 96D, 9121–9132, 1991. 9612

ACPD
11, 9607–9633, 2011

O'Connor, E. J., Hogan, R. J., and Illingworth, A. J.: Retrieving stratocumulus drizzle parameters using doppler radar and lidar, J. Appl. Meteorol., 44, 14–27, 2005. 9609, 9616

Pergaud, J., Masson, V., Malardel, S., and Couvreux, F.: A parameterization of dry thermals and shallow cumuli for mesoscale numerical weather prediction, Bound.-Lay. Meteorol., 132, 83–106, 2009. 9612

Pinty, J. P. and Jabouille, P.: A mixed-phase cloud parameterization for use in a mesoscale non-hydrostatic model: simulations of a squall line and of orographic precipitation, Preprints of Conference on Cloud Physics, Amer. Meteor. Soc., Everett, WA, 217–220, 1998. 9612

Rodts, S. M. A., Duynkerke, P. G., and Jonker, H. J. J.: Size distributions and dynamical properties of shallow cumulus clouds from aircraft observations and satellite data, J. Atmos. Sci., 60, 1895–1912, 2003. 9609

Rogers, R. R.: A short course in cloud physics, Pergamon Press, Oxford, UK, 266 pp., 1976. 9614

Seity, Y., Brousseau, P., Malardel, S., Hello, G., Bénard, P., Bouttier, F., Lac, C., and Masson, V.: The AROME-france convective scale operational model, Mon. Weather Rev., D24203, doi:10.1175/2010MWR3425.1, 2010. 9610, 9611

Skamarock, W. C.: Evaluating mesoscale NWP models using kinetic energy spectra, Mon. Weather Rev., 132, 3019–3032, 2004. 9619, 9620

Snider, J. R., Guibert, S., Brenguier, J.-L., and Putaud, J.-P.: Aerosol activation in marine stratocumulus clouds: 2. Köhler and parcel theory closure studies, J. Geophys. Res., 108(D15), 8629, doi:10.1029/2002JD002692, 2003. 9609

Zhu, P. and Zuidema, P.: On the use of PDF schemes to parameterize sub-grid clouds, Geophys. Res. Lett., 36, L05807, doi:10.1029/2008GL036817, 2009. 9616

ACPD
11, 9607–9633, 2011

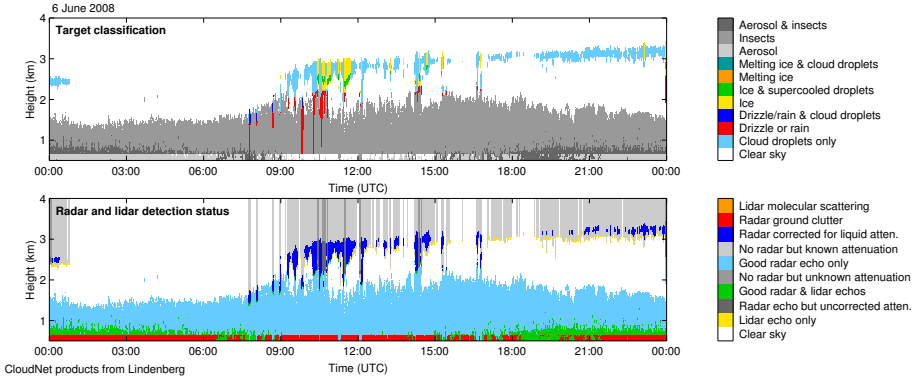

Fig. 1. Cloudnet classification product for Lindenberg on 6 June 2008.

ACPD
11, 9607–9633, 2011

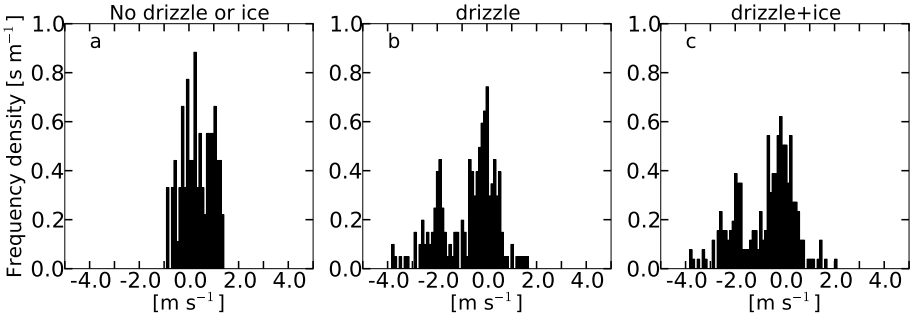

Fig. 2. Vertical velocity distributions at cloud-base for 6 June 2008 at Lindenberg demonstrating bias caused by fall speed of large particles. Left: liquid cloud droplets only, center: drizzle included, right: ice particles and drizzle included. Velocity is positive upwards.

ACPD
11, 9607–9633, 2011

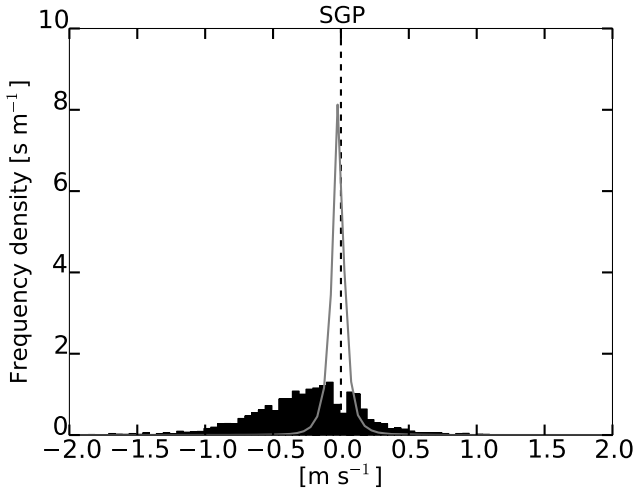

Fig. 3. Distribution of cloud-base vertical velocity at SGP in January for AROME (grey line) and CloudNet observations (filled black bars) for cloud-bases between 1000 and 1500 m. The vertical velocity bin width is 0.05 m s^{-1} for all curves.

ACPD
11, 9607–9633, 2011

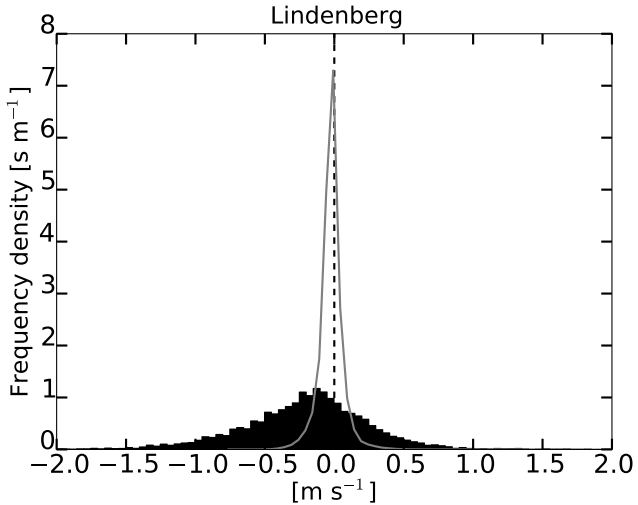

Fig. 4. Same as Fig. 3, but for Lindenberg.

ACPD
11, 9607–9633, 2011

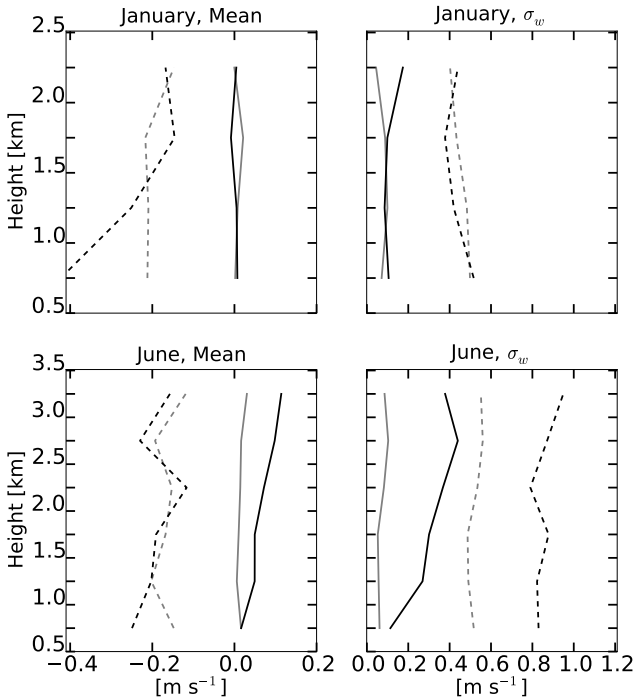

Fig. 5. Vertical velocity distribution statistics as a function of height at SGP (black) and Lindenberg (grey) for AROME (solid lines) and observations (dashed lines).

ACPD
11, 9607–9633, 2011

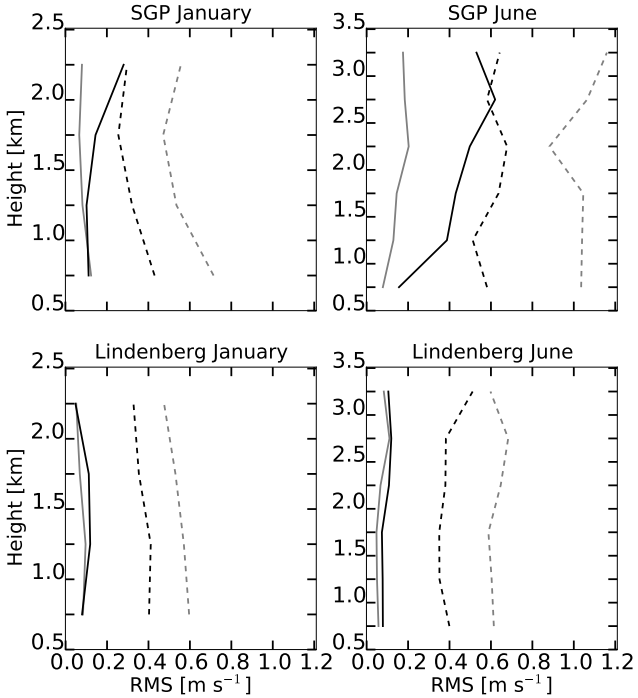

Fig. 6. Profiles of RMS-values calculated separately for negative (grey lines) and positive (black lines) parts of the vertical velocity PDFs from AROME (solid lines) and observations (dashed lines).

ACPD
11, 9607–9633, 2011

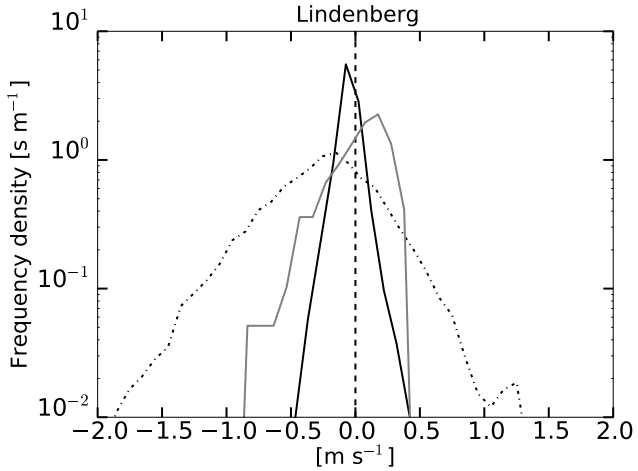

Fig. 7. Case study for Lindenberg, 29–30 January 2008: histograms of vertical velocity for AROME (solid black), observations averaged to 2500 m scale (solid grey), and observations at their original resolution (black dash-dot line). The vertical dashed line marks the 0 m s^{-1} velocity. Note the logarithmic scaling on the vertical axis. The vertical velocity bin width is 0.1 m s^{-1} for all curves.

ACPD
11, 9607–9633, 2011

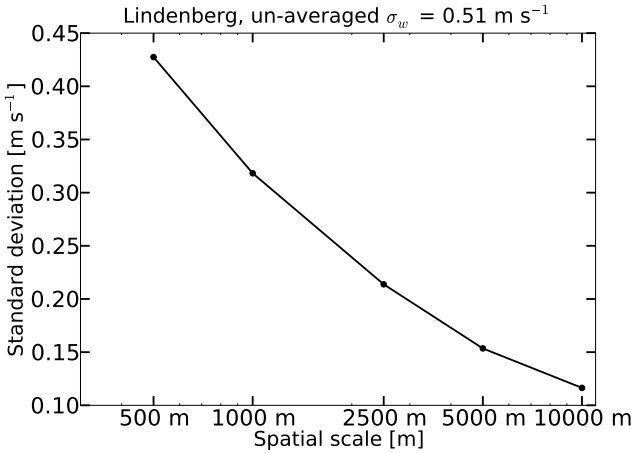

Fig. 8. Case study for Lindenberg, 29–30 January 2008: σ_w in averaged observations as a function of the spatial averaging scale.

ACPD
11, 9607–9633, 2011